First measurements of thermal neutron distribution in the LHD torus hall generated by deuterium experiments

First measurements of thermal neutron distribution in the LHD torus hall generated by deuterium experiments

Makoto Kobayashi[a], Tomoyo Tanaka[c], Takeo Nishitani[a], Kunihiro Ogawa[a,b], Mitsutaka Isobe[a,b], Akemi Kato[a], Takuya Saze[a], Sachiko Yoshihashi[c], Masaki Osakabe[a,b], and LHD Experiment Group

[a] *National Institute for Fusion Science, National Institutes of Natural Sciences, 322-6 Oroshi, Toki, Gifu, 509-5202, Japan*

[b] *SOKENDAI(The Graduate University for Advanced Studies), 322-6 Oroshi, Toki, Gifu, 509-5292, Japan*

[c] *Nagoya University, Japan, Furo, Chikusa, Aichi,464-0814 Japan*

For the estimation of the neutron field generated by deuterium plasma operation in the Large Helical Device (LHD), the first measurement of the thermal neutron distribution on the floor level of the LHD torus hall was carried out. For the thermal neutron detection, indium was used as activation foils. The radioactivity of these foils were evaluated by a high-purity germanium detector (HPGe) and an imaging plate (IP). The major components of radioactive isotope of indium was ^{116m}In. The mapping of thermal neutron distribution in the torus hall was performed. The interactions between neutron and components around LHD were observed in the thermal neutron distribution. Also, the borated polyethylene blocks effectively absorbed the thermal neutron. The thermal neutron distribution evaluated in this work can be helpful to predict the amount of radioactive waste in the torus hall proceeding with deuterium experiment in LHD.

Keywords: LHD, neutronics, activation foil, IP, HPGe

author's email: kobayashi.makoto@nifs.ac.jp

1. Introduction

In the Large Helical Device (LHD), which is one of the largest superconducting fusion plasma experimental machines, experiments using deuterium plasma (deuterium experiment) began in March 2017. In the commissioning of deuterium experiments, the control of radiation such as tritium and neutrons generated by deuterium fusion reaction is remarkably important. The annual neutron yield is permitted up to 2.1×10^{19} [1]. It is also predicted that the maximum neutron yield is 1.9×10^{16} n s^{-1}. It is well known that neutron easily penetrates almost any kind of materials and activates materials mainly by the neutron capture reaction. The activated materials emit gamma/beta rays, and this results in a radiation dose for workers. Also, those interactions of neutron occasionally produce a malfunction in highly integrated electric components such as programmable logic controller (PLC) [2,3]. For the steady operation and the maintenance of LHD, neutron transport and subsequent activation should be precisely predicted.

The activation process of neutron depends not only on the materials but also on the neutron energy. In the deuterium plasma, most of the neutrons should be generated by the fusion reaction between deuterium with the energy of 2.45 MeV. Otherwise, tritons generated by a deuteron-deuteron fusion reaction subsequently react with other deuterons, resulting in the deuteron-triton fusion reactions, which produce the 14.1 MeV neutrons. These neutrons move from LHD plasma and lose their energy by collisions with the LHD machine itself as well as with the surrounding components and the concrete walls of the experimental building. The species of radioactive isotopes in the torus hall have specific decay processes and decay rates. Some radioactive isotopes have long half-lives, and will still survive even after a long time has passed following the shutdown of LHD. The prediction of radioactivity in the torus hall proceeding with deuterium experiments is required for the future decommissioning of LHD.

Three-dimensional Monte Carlo simulation is typically used to predict the neutron behavior and the activation in system. In particular, a General Monte Carlo N-Particle Transport Code version 6 (MCNP6) has been applied for the neutronics of LHD [4,5]. The distribution and energy spectrum of neutron as well as gamma-ray in the torus hall

author's email: kobayashi.makoto@nifs.ac.jp

and the basement of the LHD experimental building have been calculated and reported elsewhere [5]. For the further development of neutronics calculation, the actual measurement of neutron distribution is quite important as it provides the answer of neutron transport and guarantees the validity of calculation.

Therefore, as the first actual measurements, the neutron distribution on the floor level of the LHD torus hall was evaluated in this work. Activation foils of indium were applied. The radioactivity of indium foils, which correlates with the neutron fluence across the foil, was evaluated by means of a high-purity germanium detector (HPGe) and an imaging plate (IP). This is the first measurement of neutron distribution in the torus hall of a large helical type fusion device, and will be an important benchmark for safety evaluation for the deuterium experiment in LHD.

2. Experiments and analyses

2.1 The component layout of the LHD torus hall

The torus hall of LHD is on the first floor of the LHD experimental building. The torus hall has the size of W75, L45, and H40 m^3, and is made of concrete wall with the thickness of 2 m to sufficiently shield radiation. The details of the component layout in the torus hall can be found in Fig. 1. LHD is placed slightly to the east side of the torus hall. The vacuum vessel of LHD is surrounded by the 2 helical coils and 6 poloidal field coils, and they are covered by the cryostat. The space between the vacuum vessel and the cryostat is evacuated to an ultra-high vacuum to prevent the air exposure to the surface of coils because the temperature of coils must be maintained in low temperature around 4 K.

Many systems are equipped to LHD and serve for heating plasma, diagnostics of plasma, and other purposes. One of the large heating systems in LHD is NBI. There are 5 NBIs for LHD. Three of them are tangential NBI (#1, #2, #3) and the two others are radial NBI (#4, #5).

The borated polyethylene blocks working as neutron shielding materials were widely used in LHD. Polyethylene can effectively decelerate fast neutron from LHD to thermal neutron due to its light constituent atoms. Then, boron inside the polyethylene blocks

absorbs thermal neutrons by its large cross-section of $^{10}B(n,\alpha)^{7}Li$ reaction. The borated-polyethylene blocks contain 10 % boron. Many electrical components in the torus hall were covered with borated polyethylene blocks. In addition, on the floor underneath LHD, the borated polyethylene blocks were placed like a disc with the inner radius of ~ 2.3 m, outer radius of ~ 6.9 m, and the thickness of 5 cm to reduce the radioactivity of the concrete floor underneath LHD. Exceptionally, un-borated polyethylene blocks were used just below the 8-O port of LHD, which is the west side of LHD as seen in Fig. 1, and they occupied 36 degrees of disc-shaped polyethylene blocks underneath LHD.

2.2 Neutron sources and diagnostics

The major source of neutron should be deuterium plasma in LHD. In the vacuum vessel of LHD, the deuterium plasma with the major radius of about 3.75 m will be generated. During this plasma operation (usually for 3 seconds), neutrons will be produced. Note that, neutron yields in each deuterium plasma operation are different because they depend on the many plasma parameters such as temperature, density, magnetic field, and others.

The other neutron source will be NBI. In NBI, the ions of hydrogen isotopes are accelerated and then neutralized in order to have hydrogen isotopes penetrate into plasma confined by the magnetic field. In this extraction process of neutral beam, not all hydrogen isotope ions are neutralized. These ions are guided by the magnetic force into the inner wall of the NBI system as a beam dump. In this time, deuterons in the ion beam collide with deuterium retained in the beam dump. Consequently, neutron will be generated. In the present study, hydrogen was used for tangential NBI. Deuterium was used in radial NBI. Therefore, the neutron generation was expected in NBI#4 and NBI#5.

Neutron yield was measured by the neutron flux monitors (NFM), which were placed at the top of the LHD center axis (#1) and around the vacuum port of LHD on the mid plane (#2, #3). The ^{235}U fission chambers, ^{10}B counters, and ^{3}He counters were adopted as NFM in LHD. The positions of NFM are also added into Fig. 1.

2.3 Activation foils

As the activation foil, indium (In) was selected in this work. The advantages of using indium foils are (i) high reaction cross-section with neutron, (ii) short half-life of radioactive isotopes and (iii) with selective reaction by neutron energy [6]. Indium was used in this work to measure fast and thermal neutrons individually at one time due to the third advantage above. The natural isotopes of indium are ^{113}In and ^{115}In. The natural abundances of these indium isotopes are 4.3 % and 95.7 %, respectively. Thermal neutrons react with ^{115}In as ^{115}In(n,γ)^{116m}In. The cross-section of this reaction is 201.2 barn for the 0.025 eV neutron. The minor isotope of indium as ^{113}In also reacts with thermal neutron as ^{113}In(n, γ)^{114m}In. The cross-section is 12.1 barn for the 0.025 eV neutron. Besides, fast neutrons can only react with ^{115}In as ^{115}In(n,n')^{115m}In. The cross-section of this (n,n') reaction was about 2 barn for 2.45 MeV neutron. This reaction requires higher neutron energy than the threshold energy of 0.3 MeV in order to occur. Therefore, the radioactivity of ^{115m}In presents only fast neutron fluence. The details of cross-sections for the above 3 reactions can be found in Ref. [7]. The half-lives of ^{114m}In, ^{115m}In and ^{116m}In are 49.5 days, 4.49 hours and 54.3 minutes, respectively. Therefore, ^{116m}In decays faster than others, and ^{114m}In only exists in indium foils after several days have passed.

The radioactivity of the activation foil does not directly present the neutron fluence at the position of the foil, as the foil has been exposed to various neutron environments with different fluxes and experienced the decay of radioactive isotopes during neutron irradiation. The amounts of radioactive isotopes produced during neutron irradiation can be calculated simply by the following equation,

$$\frac{dN^{(A)}}{dt} = N^{(S)}\sigma\phi - \frac{ln2}{T_{\frac{1}{2}}}N^{(A)} \quad (1).$$

Here, $N^{(A)}$ and $N^{(S)}$ are the amounts of radioactive and stable isotopes [-], respectively, and ϕ presents the neutron flux [cm^{-2} s^{-1}] and $T_{1/2}$ is half-life [s]. The reaction cross-section, σ [cm^2] is dependent on the neutron energy. The $N^{(A)}$ is zero before the neutron irradiation. The half-lives of radioactive isotopes of indium are as found above. Note that, ϕ is different in each deuterium plasma operation, and $N^{(A)}$ is determined by the

integration of these different neutron fields. On the other hand, the source and the energy of neutron are the same in every deuterium plasma operation.

According to Eq. 1, the history of the neutron yield and the reaction cross-section are necessary to evaluate the neutron flux from the radioactivity of the foil. In this work, the history of the neutron yield was obtained by NFM. The reaction cross-section was estimated by MCNP6 code with using the nuclear data library of ENDF/B-VII.1 [6].

2.4 Estimation of nuclear reaction cross-section

The model for MCNP6 calculation used in this work includes LHD, the cryostat, the torus hall and the basement of the torus hall [5]. Pipes and ducts between the torus hall and the basement were also taken into account. The polyethylene blocks underneath LHD, which was explained in the Section 2.1, were also considered. The helical surface of LHD was modeled as a combination of 6-degrees toroidal angle sections to make a helical shape torus. Also, the helical coils, poloidal field coils, vacuum ports, helium coolant channels were installed in the model. This model for MCNP6 calculation has been already applied for the calibration of NFM in LHD, and the detail of this model can be found in Ref. [5].

The source of neutron was modeled as isotropic distribution in the same shape of the plasma. The source neutron energy was assumed to be 99.5 % of 2.45 MeV and 0.5 % of 14.1 MeV according to the previous work [8].

The reaction cross-section was calculated by the above model with using mesh tally in MCNP6. The calculation was performed until the statistical error became less than 0.1.

2.5 Exposure to neutron in the LHD torus hall

Regarding the routine weekly operation of LHD, the first weekday is assigned for maintenance, and the other weekdays are designated for experiment. The samples were placed on the floor of the LHD torus hall on the maintenance day (April 10, 2017). To cover the floor of the LHD torus hall (45 × 75 m), most of the samples were distributed

far enough apart from each sample with the distance of about 2~3 m. The positions where the samples were set are presented in Fig. 4 as red colored circles or stars.

Deuterium plasma experiments were carried out on the next day (April 11, 2017). The experiments started from around 10:00 and continued up to 18:00. Fig. 2 shows the neutron yield of 128 shots in total in this day. During deuterium plasma experiments, it was confirmed that there was no person in the LHD torus hall. Therefore, all samples were kept in the LHD torus hall until the experiments finished. After a daily plasma operation finished, and a pause to have the radiation dose in the LHD torus hall reduced, all samples were salvaged.

2.6 Analyses of radioactivity

As the radioactive isotopes of indium emit gamma-rays, two analysis methods were used to measure the radioactivity of samples. One of them was HPGe, which can identify the radioactive isotopes by gamma-ray energy spectrometry, and is widely used in the field of radiation control. HPGe also can evaluate the precise quantity of radioactive isotopes. However, this usually requires a longer time, and needs to measure samples one by one. The other method was IP. IP is a sheet-type detector which can store the energy transferred from radiation. IP can release the integrated stored-energy as photo-stimulated luminescence (PSL) by laser injection. IP is usually applied for two-dimensional visualization of the radiation source as it has the capability to measure for a large area surface. The errors of radioactivity which were evaluated by HPGe and IP measurements were less than 5 % and 10-20 %, respectively.

Samples after salvaging were mounted on the mylar film with the thickness of 100 μm and were placed on IP. Then, IP measurements were carried out intermittently (chronological measurement). The IP measurements were continued up to the time when the PSL is undetectable or unchanged with elapsed time. A small number of samples were taken out from mylar film and measured by HPGe for the gamma-ray spectrometry. The details of these analyses were described in our previous work [9].

3. Results and discussion

Fig. 3 shows the results of chronological IP measurements for indium samples. The starting time of this measurement (Elapsed time = 0 min) corresponds to about 3 hours after the last deuterium plasma shot. The length in the legend of this figure indicates the distance of sample position from the central position of LHD toward the west wall. For example, the position with a distance of 0 m indicates the central position of LHD. As shown in Fig. 3, the time trend of the PSL integration rate showed two phased decreases. The first stage, which is between the elapsed time around 0-500 min, showed an exponential decrease. The exponential factor of first stage were almost the same in these samples. This fact indicates that the major component of radioactive indium isotope in these samples should be the same. According to the exponential fitting for these time-trends of PSL integration rate, the exponential factors in the first stage were around -1.2 ~ -1.5 min^{-1}. From the decay process of radioactive isotopes, these exponential factors are equivalent to $-\ln 2/T_{1/2}$. Therefore, the half-life in the first stage was around 50 min, which is close to the half-life of ^{116m}In [10]. ^{116m}In as the major radioactive isotope of indium samples was also confirmed by the gamma-ray spectrometry measured by HPGe.

As discussed in Section 2.3, it had been expected that there would be three phased decrement stages in chronological IP measurement. Indeed, the three phased decrease of PSL integration rate with elapsed time were found in our previous work for fast neutron irradiated indium [9]. However, Fig. 3 showed the two phased decrease. The lower and unchanged PSL after a long time elapsed would suggest the presence of ^{114m}In. The radioactivity of ^{115m}In which can evaluate fast neutron fluence could not be measured in this work. This is because of the relatively lower cross-section of ^{115}In(n,n')^{115m}In reaction compared to others. Therefore, only thermal neutron distribution was elucidated in this work. The measurements for the distribution of fast neutron as well as epi-thermal neutron are now planned with using different activation foils and thermal neutron absorber such as nickel, gold, and cadmium, respectively.

The radioactivity of ^{116m}In at the start time of IP measurements are summarized as Table 1. The radioactivities of ^{116m}In were almost similar between 0-6 m, and between 21-43 m. The former region is underneath LHD, and the latter region is near the open space of the torus hall which is for maintenance work. The radioactivity of ^{116m}In in the former region was more than 10 times as large as that in the latter region. For the latter

region, the thermal neutron distribution would be almost uniform although the distance from LHD is significantly different between these two positions (21-43 m).

Fig. 4 shows the distribution of thermal neutron flux on the floor level of the LHD torus hall measured in this work. In this figure, the thermal neutron flux when one neutron generates in LHD per 1 s was defined as ε_{th} [cm^{-2} s^{-1}], and displayed. This figure was constructed by using Generic Mapping Tool (GMT) version 5.4.3. The red points in this figure indicate the position of indium foil. As the distances among samples were not so close, the distribution resembles a blur. However, the overall tendency of thermal neutron distribution can be found in this figure. The thermal neutron flux was relatively high around LHD. In particular, the higher thermal neutron flux was observed at the central position and underneath the 8-O port of LHD. The polyethylene blocks were absent in the center part of LHD. Fast neutrons from LHD would be thermalized effectively in the concrete floor as it contains a large amount of water. Also, the un-borated polyethylene blocks were placed underneath the 8-O port of LHD. Because of the absence of boron in blocks, the fast neutron effectively converted to thermal neutron. Conversely, the combination of polyethylene and boron reduced the activation of components effectively, because relatively lower thermal neutron flux was observed underneath LHD except the above two positions.

It was also found that the thermal neutron distribution changed with the components near LHD. For example, thermal neutron flux backside of NBI against LHD became lowered, especially, around NBI#2, NBI#3 and NBI#4. Also, thermal neutron flux was lowered around the power supply systems of NBI, which are placed behind the NBI against LHD. This would be caused by the shielding of thermal neutron by the components around LHD. Neutrons would also generate in the beam dump of NBI system. However, a significant thermal neutron distribution around NBI was hardly observed. It can be expected that the neutron generated in LHD would dominate the overall distribution of thermal neutron in the torus hall. This result is consistent with the previous expectation that the neutron yield in NBI is three orders of magnitude as low as that in LHD [1].

In the region near the wall of the torus hall, thermal neutron flux was about one order of magnitude as low as that near LHD. The distribution of thermal neutron was

almost uniform in this region. Because of the absence of components around the wall, the thermal neutron would be able to move without large absorption process. This would be a reason for the almost uniform thermal neutron distribution near the wall in the torus hall.

The evaluation of thermal neutron distribution on the floor level of the LHD torus hall was carried out successfully with using indium foils at the first time during deuterium experiment. The thermal neutron distribution visualized in this work were well reflected with the deceleration, shielding and absorption of neutron by the components in the torus hall. Because only two kinds of neutrons (2.45 MeV neutron and 14.1 MeV neutron) would be generated in the LHD plasma and the ratio of these neutrons would not largely change, the distribution obtained in this work will be available for the future operation. According to these results, the prediction of radioactivity in LHD body, components, as well as concrete wall proceeding with deuterium experiments are ongoing for the decommissioning of the torus hall.

However, the thermal neutron distribution obtained here was only on the floor level. The three-dimensional distribution of thermal neutron would be necessary. Also, the distribution of fast neutron could not be evaluated in this work. The estimation of fast neutron distribution will be important because fast neutrons can penetrate deeper regions of thick material such as concretes, and produce radioactivity inside. The evaluation of fast neutron flux distribution will be planned with using other activation foils such as nickel in future.

4. Conclusion

For the estimation of the neutron field generated by deuterium plasma operation in LHD, the first measurement of the thermal neutron distribution on the floor level of the LHD torus hall was carried out. Indium was used as activation foils, and the radioactivity of these foils were evaluated by HPGe and IP. The major components of radioactive isotope of indium was ^{116m}In. The mapping of thermal neutron distribution showed the interactions between neutron and components around LHD. The borated polyethylene blocks effectively absorbed thermal neutron. The thermal neutron flux

near the concrete wall of the torus hall would be approximately one order of magnitude lower than that near LHD. The thermal neutron distribution evaluated in this work will be helpful to predict the amount of radioactive waste in the torus hall proceeding with deuterium experiment.

Acknowledgments

This work was supported by LHD project budget (ULGG801). The authors wish to thank the LHD Technical Group for their assistance in this work.

References

[1] M. Osakabe, Y. Takeiri, T. Morisaki, G. Motojima, K. Ogawa, M. Isobe, M. Tanaka, S. Murakami, A. Shimizu, K. Nagaoka, H. Takahashi, K. Nagasaki, H. Takahashi, T. Fujita, Y. Oya, M. Sakamoto, Y. Ueda, T. Akiyama, H. Kasahara, S. Sakakibara, R. Sakamoto, M. Tokitani, H. Yamada, M. Yokoyama, Y. Yoshimura & LHD Experiment Group, Current Status of Large Helical Device and Its Prospect for Deuterium Experiment, Fusion Sci. Technol., **72** (2017) 199-210.

[2] K. Ogawa, T. Nishitani, M. Isobe, I. Murata, Y. Hatano, S. Matsuyama, H. Nakanishi, K. Mukai, M. Sato, M. Yokota, Investigation of irradiation effects on highly integrated leading edge electronic components of diagnostics and control systems for the LHD deuterium operation, Nucl. Fusion, **57** (2017) 086012.

[3] K. Ogawa, T. Nishitani, M. Isobe, M. Sato, M. Yokota H. Hayashi, T. Kobuchi, T. Nishimura, Effects of gamma-ray irradiation on electronic and non-electronic equipment of Large Helical Device, Plasma. Sci. Technol, **19** (2017) 025601.

[4] X-5 Monte Carlo Team, MCNP User's Guide - Code Version 6.1.1beta, LA-CP-14-00745 (Los Alamos National Laboratory, Los Alamos, 2014)

[5] T. Nishitani, K. Ogawa, H. Kawase, N. Pu, T. Ozaki, M. Isobe, Monte Carlo calculation of the neutron and gamma-ray distributions inside the LHD experimental building and shielding design for diagnostics, accepted to Prog. Nucl. Sci. Technol.

[6] K. Shibata, O. Iwamoto, T. Nakagawa, N. Iwamoto, A. Ichihara, S. Kunieda, S. Chiba, K. Furutaka, N. Otuka, T. Ohsawa, T. Murata, H. Matsunobu, A. Zukeran, S. Kamada, and J. Katakura, JENDL-4.0: A New Library for Nuclear Science and Engineering, J. Nucl. Sci. Technol. **48** (2011) 1-30.

[7] M.B.Chadwick, M.Herman, P.Obložinský, M.E.Dunn, Y.Danon, A.C.Kahler, D.L.Smith, B.Pritychenko, G.Arbanas, R.Arcilla, R.Brewer, D.A.Brown, R.Capote, A.D.Carlson, Y.S.Cho, H.Derrien, K.Guber, G.M.Hale, P.G.Young, ENDF/B-VII.1 Nuclear Data for Science and Technology: Cross Sections, Covariances, Fission Product Yields and Decay Data, Nuclear Data Sheets **112** (2011) 2887-2996.

[8] T. Nishitani, K. Ogawa, I. Isobe., Monte Carlo simulation of the neutron measurement for the Large Helical Device deuterium experiments, Fusion Eng. Des., **123** (2017) 1020-1024.

[9] M. Kobayashi, T. Nishitani, A. Kato, T. Saze, T. Tanaka, S. Yoshihashi, K. Ogawa, M. Isobe, Evaluation of imaging plate measurement for activated indium as fast-neutron detector in large radiation field, accepted to Prog. Nucl. Sci. Technol.

[10] R. B. Firestone, Table of isotopes 8th edition, John Wiley & Sons, Inc. 1996.

Figure captions

Table 1 The radioactivities of ^{116m}In and the thermal neutron fluxes at the center position of LHD toward the west direction.

Fig. 1 Component layout of the LHD torus hall

Fig. 2 History of neutron yield measured by LHD-NFM

Fig. 3 PSL integration rate measured by IP for indium foils placed at center position of LHD toward the west direction

Fig. 4 The thermal neutron flux distribution on the floor level of the LHD torus hall measured by activation foils. The contour color was made by the GMT default rainbow color palette in the range of -7.2(red) ~ -9.8(purple). Red circles in Fig. 4 indicate the position of sample. Red stars also indicate the position of samples used in Fig. 3.

Table 1 Makoto Kobayashi et al.

Position from LHD center (m)	**0**	**6**	**13**	**21**	**43**
Radioactivity of ^{116m}In in a foil (Bq g^{-1})	1.5×10^{4}	1.7×10^{4}	4.6×10^{3}	7.5×10^{2}	4.2×10^{2}
Thermal neutron flux ε (cm^{-2} s^{-1})	2.5×10^{-8}	3.3×10^{-8}	1.0×10^{-8}	1.8×10^{-9}	1.0×10^{-9}

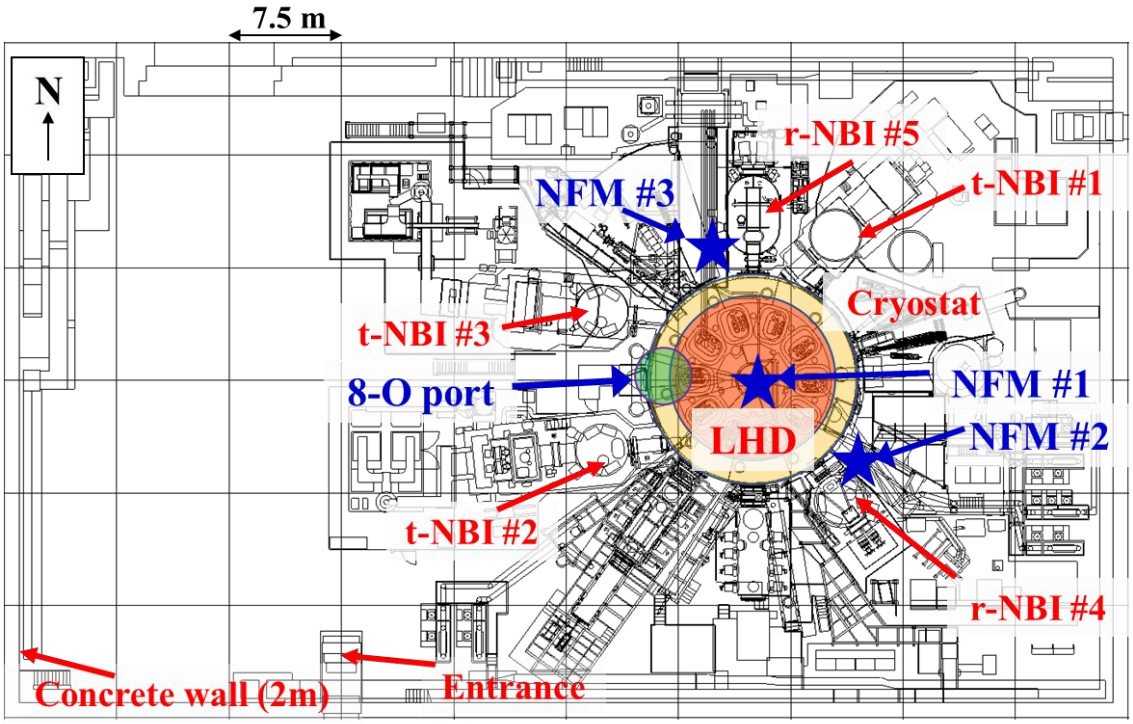

Fig. 1 Makoto Kobayashi et al.

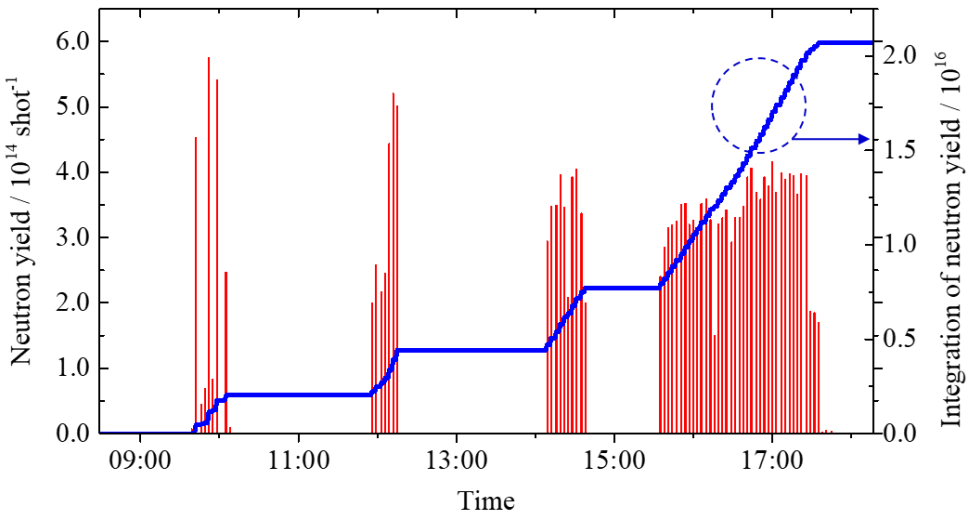

Fig. 2 Makoto Kobayashi et al.

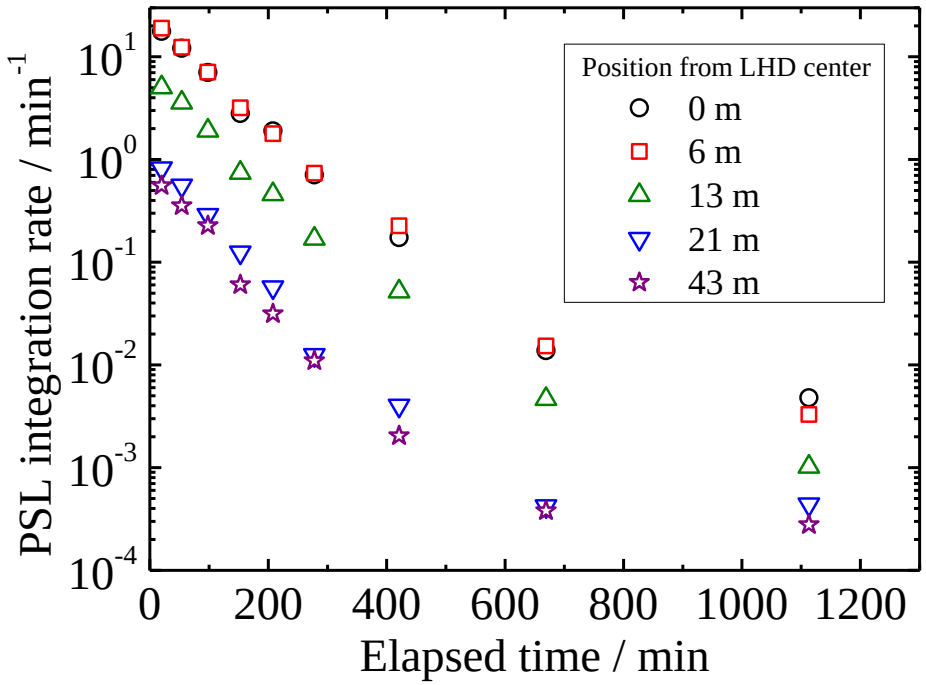

Fig. 3 Makoto Kobayashi et al.

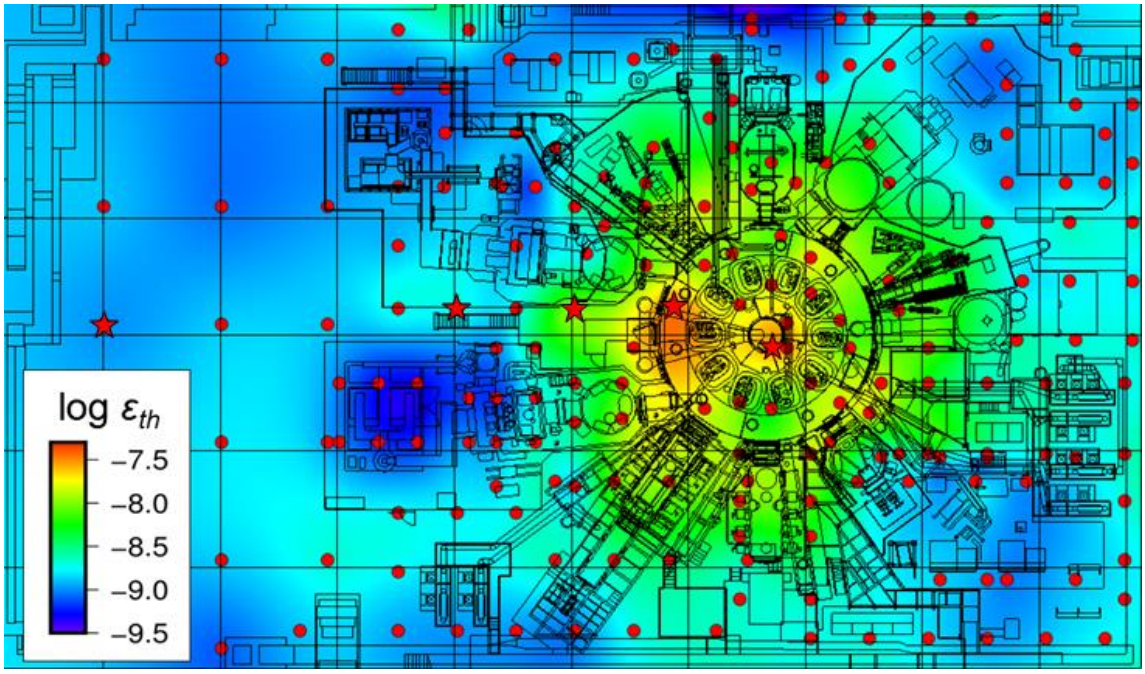

Fig. 4 Makoto Kobayashi et al.